Available online at www.sciencedirect.com
ScienceDirect
International Journal of Mass Spectrometry 255–256 (2006) 265–278
International Journal of Mass Spectrometry
www.elsevier.com/locate/ijms

The fragmentation of protonated tyrosine and iodotyrosines: The effect of substituents on the losses of NH_3 and of H_2O and CO☆

Junfang Zhao, Tamer Shoeib [1], K.W. Michael Siu, Alan C. Hopkinson *

Department of Chemistry and Centre for Research in Mass Spectrometry, York University, 4700 Keele Street, Toronto, Ont., Canada M3J 1P3

Received 21 December 2005; received in revised form 20 March 2006; accepted 20 March 2006
Available online 25 April 2006

Abstract

The gas-phase dissociation chemistries of protonated 3-iodo-L-tyrosine, 3,5-diiodo-L-tyrosine and 3,3′,5,5′-tetraiodo-thyronine (thyroxine) have been examined using a combination of tandem mass spectrometry and density functional theory (DFT) calculations. It was found that, at low collision energy, all protonated tyrosines exhibit common fragmentation pathways, including the competitive eliminations of NH_3 and the concomitant loss of H_2O and CO, but there are significant differences in relative abundances, depending on the combined electron-donating abilities of the substituents in the phenyl ring. The ions initially formed by loss of NH_3 are phenonium ions, but subsequent fragmentation is most easily understood in terms of the isomeric benzyl cation structures. These $[M+H-NH_3]^+$ ions fragment at relatively low collision energies, mainly by loss of ketene; by contrast, the $[M+H-H_2O-CO]^+$ ions are more stable towards dissociation. At higher collision energies, losses of one, two and even three iodine atoms were observed. DFT calculations (at the B3LYP/DZVP level of theory) were performed on protonated 3-iodotyrosine to compare the reaction profiles for the fragmentation mechanisms. The iodo-substituent in the 3-position is weakly electron-withdrawing and this results in a barrier (27.5 kcal/mol at 0 K) that is slightly higher than that for protonated tyrosine (26.8 kcal/mol). The phenoxy group PhO– is a weaker electron-donor than HO– and protonated 3,5-diiodo-4-phenoxytyrosine has an even higher barrier (31.1 kcal/mol) to NH_3 loss than protonated 3,5-diiodotyrosine (28.8 kcal/mol). Linear free energy plots for $\Delta H_0^{\circ\ddagger}$ and $\Delta G_{298}^{\circ\ddagger}$ against σ^+ for the four protonated tyrosine derivatives show good correlations. More importantly, as the products of the dissociation are higher in energy than the transition states to their formation, the plots of ΔH_0° and ΔG_{298}° for the overall reaction for NH_3 loss also correlate very well with σ^+ (correlation coefficients of 0.99 and 0.98, respectively). The positive slopes of these Hammett plots show that the barriers to the loss of NH_3 by the neighboring-group mechanism are increased by the presence of electron-withdrawing groups in the phenyl rings.

Keywords: Collision-induced dissocation; Density functional calculation; Substituent effect; Hammett plot; Protonated thyroxine

1. Introduction

Collision-induced dissociation (CID) of protonated peptides in tandem mass spectrometry has become an important technique for determining amino acid sequences. Soft ionization methods such as electrospray ionization (ESI) [1] and matrix-assisted laser desorption/ionization (MALDI) [2] produce protonated proteins or peptides and the fragmentation products that these ions yield under CID conditions can be used to determine the amino acid sequences of the precursor ions [3–9]. There have been many experimental [10–21] and theoretical [22–26] studies of the mechanisms by which protonated peptides fragment. These have raised basic questions about how protonated α-amino acids, the building blocks of peptides, fragment and there have been several studies of the fragmentation pathways of protonated α-amino acids [27–34].

Protonated aliphatic α-amino acids fragment predominantly to form their respective iminium ions by concomitant loss of H_2O and CO, giving rise to very simple CID mass spectra. Hydroxylic and acidic α-amino acids have OH and COOH groups in their side chains and these, in addition to the concomitant loss of H_2O and CO, also lose H_2O from the side chain. The favored site of protonation of the basic α-amino acids, arginine and lysine, is a nitrogen on the side chain [35] and their dominant fragmentation pathways involve loss of NH_3 and, in the case

☆ In honour of Diethard Kurt Bohme, in recognition of his major contributions in the areas of mass spectrometry, gas-phase ion chemistry and thermochemistry.

* Corresponding author. Tel.: +1 416 736 2100x77839; fax: +1 416 736 5936.
E-mail address: ach@yorku.ca (A.C. Hopkinson).
[1] Institute for National Measurement Standards, National Research Council of Canada, Ottawa, Ontario, Canada K1A 0R9.

1387-3806/$ – see front matter © 2006 Elsevier B.V. All rights reserved.
doi:10.1016/j.ijms.2006.03.012

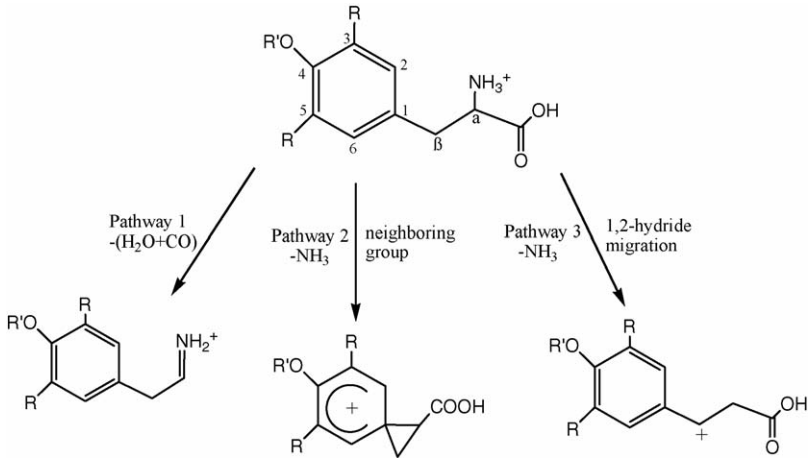

Scheme 1.

of protonated arginine, guanidine [27,28]. Aromatic α-amino acids, with the exception of protonated histidine, exhibit facile elimination of NH_3, in addition to the concomitant elimination of H_2O and CO [27,30,36–39]. At higher collision energies, eliminations of H_2O, CO, CO_2 and CH_2CO occur after that of NH_3 and eliminations of HCN, $HCNH_2$, and NH_3 occur after that of H_2O and CO [30]. In addition, aromatic α-amino acids, with the exception of tyrosine, were observed to yield cationic radical fragments by eliminating small radicals, including $H^{\bullet}$, $CH_3^{\bullet}$, and $NH{=}CH^{\bullet}$ [30].

Facile losses of the α-amino group as ammonia are believed to involve neighboring-group participation, a reaction in which a nucleophile in the side chain attacks the α-carbon displacing the protonated amino group as NH_3. Attack by the ipso-carbon of the phenyl group of protonated phenylalanine can displace NH_3 to form a phenonium ion [27,36,37], attack by the sulfhydryl group of protonated cysteine facilitates loss of NH_3 to form an episulfonium ion [31], and attack by C3 of protonated tryptophan forms a spirocyclopropane intermediate, the indolenyl equivalent of the phenonium ion [32]. Fragmentation of protonated tyrosine results in higher abundances of the $[M+H-NH_3]^+$ than that of the corresponding product from protonated phenylalanine, and this has been attributed to the ability of the *p*-hydroxy group to stabilize the transition state on the pathway to formation of the phenonium ion. Very recently, Lioe and O'Hair [37] investigated neighboring-group processes in the deamination of a series of protonated phenylalanines in which various substituents (NH_2, OH, OCH_3, CH_3, Cl, Br, I, CN, and NO_2) were substituted in the phenyl ring. Protonated phenylalanines bearing electron-withdrawing groups were found to favor the concomitant loss of H_2O and CO; by contrast, electron-donating substituents promoted the loss of NH_3.

The α-amino nitrogen is the preferred site of protonation for aromatic amino acids [35] and the highest barrier to the concomitant loss of H_2O and CO is for the intramolecular migration of a proton from the NH_3^+ to the OH of the COOH group [37–42] (pathway 1, Scheme 1). The activation energies for this unimolecular dissociation reaction for a series of protonated *p*-X-phenylalanines were found to be largely independent of the substituent [37].

In principle, there are two plausible internal displacement mechanisms by which NH_3 can be lost from a protonated pheylalanine. Either the phenyl group undergoes a 1,2-shift forming the phenonium ion (pathway 2), or a 1,2-hydride shift from the benzylic CH_2 displaces the NH_3 thereby generating a benzyl cation, X–Ph–$CH^+CH(NH_2)$COOH (pathway 3). The benzyl cations have lower energies than the isomeric phenonium ions, but the barriers to formation of the benzyl cations are higher than those for formation of the phenonium ions. Activation energies for formation of the phenonium ions, calculated at B3LYP/6-31+G(d,p) [37], correlate well with the Brown–Okamoto σ^+ substituents [43], with a large negative ρ value, indicating that electron-donating substituents strongly facilitate this reaction.

Our interest here is in the fragmentation of protonated thyroxine (3,5,3′,5′-tetraiodo-thyronine) and, to aid in the interpretation of the CID spectra, we have examined tyrosine derivatives that have iodine substituents adjacent to the hydroxyl group in the phenyl ring. There has been one recent related mass spectrometry study on iodothyrones, an electrospray-ionization study of the negative ions of thyrones containing various combinations of iodo-substituted thyrones [44].

The first reported, naturally occurring, halogenated organic compound was 3,5-diiodotyrosine, isolated in 1896 from the coral, *Gorgonia cavolinii* [45]. Iodine is now considered an essential mineral in the human body and 3,5-diiodotyrosine has been shown to be the second stage of iodine incorporation into the amino acid tyrosine in the thyroid glands. The action of the enzyme thyroid peroxidase on tyrosine in the presence of iodine first produces 3-iodotyrosine, which is the precursor to 3,5-diiodotyrosine. Two 3,5-diiodotyrosine molecules then combine in the presence of this same enzyme to generate 3,5,3′,5′-tetraiodothyronine, commonly known as thyroxine, which is synthesized by invertebrates and algae [46].

Here, we provide a detailed study of the gas-phase CID products of protonated 3-iodo-L-tyrosine, 3,5-diiodo-L-tyrosine and thyroxine. The iodo-substituents in the 3-position are weakly electron-withdrawing and, assuming additivity of substituent effects, are likely to raise the barrier to loss of NH_3 (relative to that in protonated tyrosine). Furthermore, the phenoxy group PhO– is a weaker electron-donor than HO– (σ^+ is −0.50

compared with −0.92 for OH [47]) and protonated thyroxine is, therefore, expected to have an even higher barrier to NH_3 loss than protonated 3,5-diiodotyrosine. Postulated mechanisms for the subsequent dissociation pathways are examined and supported by deuterium-labeling experiments and by density functional theory (DFT) calculations.

2. Experimental

2.1. Materials

3-Iodo-L-tyrosine (99%), 3-5-diiodo-L-tyrosine (98%) and 3,3′,5,5′-tetraiodo-thyronine (97%) used in the study were commercially available from Aldrich Chemical Corporation (St. Louis, MO). Sample solutions were typically 0.1 mM in a mixture of 1:1 (v/v) H_2O/CH_3OH. Deionized water and reagent grade methanol (Aldrich) were used as solvents. Hydrogen/deuterium exchange experiments were carried out using deuterium oxide and CH_3OD (both 99.8% D, Acros organics) as solvents instead of water and methanol.

2.2. Mass spectrometry

Experiments on protonated 3-iodotyrosine were performed on a TSQ Quantum triple quadrupole and a LCQ Ion Max ion trap; both are ThermoElectron (San Jose, California) mass spectrometers. Sample solutions were continuously infused at a rate of 4 μL/min into the pneumatically assisted electrospray probe using dry nitrogen as the nebulizer gas. Mass spectra obtained on the triple quadrupole instrument were produced in the positive ion detection mode with unit (FWHM = 0.7) resolution, with a step size of 0.1 *m/z* unit at 10 ms/step. Typically not less than 10 scans were summed to produce a mass spectrum. Product and precursor ion spectra were obtained using argon as the collision gas at a pressure of about 3 mTorr. For the acquisition of product ion spectra center-of-mass collision energies (E_{cm}) in the range of 0.5–5 eV were employed; for precursor ion spectra laboratory collision energies (E_{lab}) between 5 and 50 eV were typically used.

The LCQ Ion Max auto-tune routine was used to obtain settings for lens, quadrupole and octapole voltages for maximum transmission of the ions of interest. Helium gas admitted directly into the ion trap was used as the bath/buffer gas to improve the trapping efficiency and as the collision gas for CID experiments. Experiments designed to elucidate reaction pathways were performed as follows: the ion of interest was selected with an isolation width set to 1.5 *m/z* units, collisional activation was introduced by setting the activation amplitude (which defined the amplitude of the radio frequency (RF) voltage applied to the end-cap electrodes) at 25–35% of the maximum voltage available (determined empirically), and the activation Q setting (used to adjust the frequency of the RF-excitation voltage placed on the end-caps) was set at 0.25 unit.

CID data for protonated 3,5-diiodotyrosine and thyroxine were obtained on a prototype triple-quadrupole mass spectrometer of API 3000 (MDS SCIEX, Concord, Canada). The concentrations of the sample solution were 100 μM in 50/50 methanol/water (v/v). Samples were continuously introduced into the pneumatically assisted electrospray source at a flow rate of 3.0 μL/min by a means of a syringe pump. Dry air was

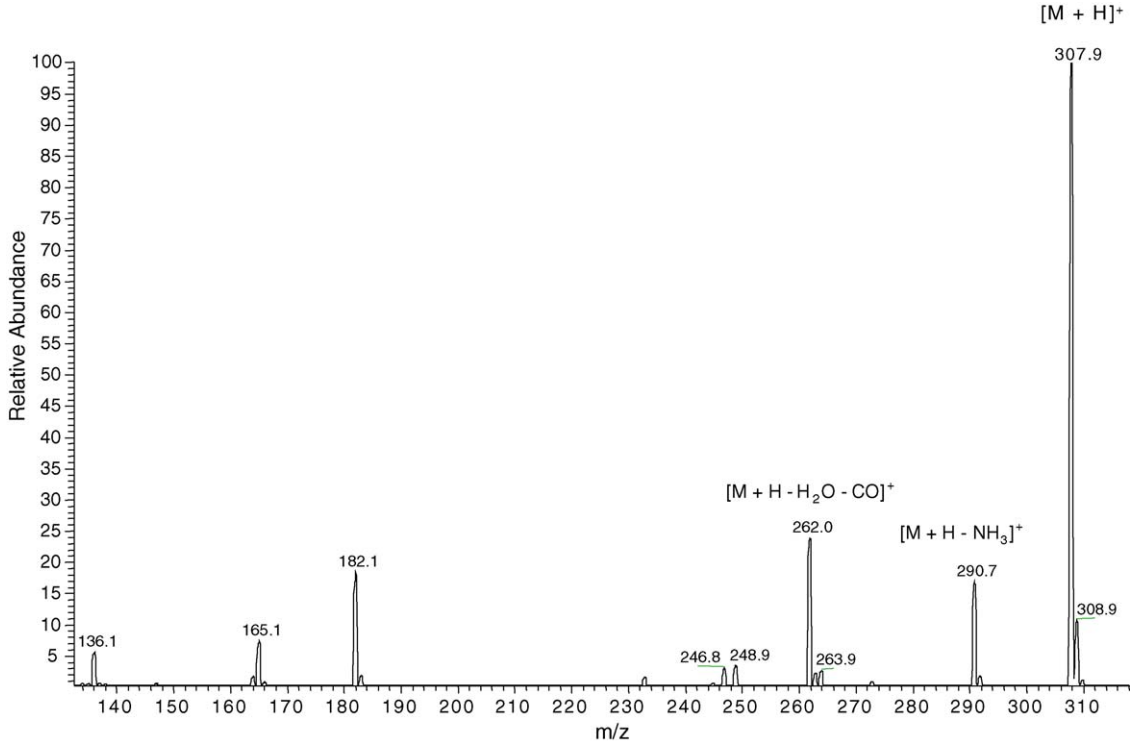

Fig. 1. Electrospray mass spectrum of protonated 3-iodotyrosine.

used as the nebulizing gas and nitrogen was used as the curtain and collision gases. Mass spectra were acquired in the positive ion detection mode with unit-mass resolution.

3. Computational methods

DFT calculations were performed using Becke's three-parameter exchange functional [48,49] and the correlation functional of Lee et al. [50] built into the Gaussian 98 program [51]. All calculations employed a double-zeta plus polarization basis set (DZVP) [52,53]. Structures were characterized by vibrational frequency calculations as being either at minima or first-order saddle points; for the latter structures, the two minima associated with the transition states were obtained by performing intrinsic reaction coordinate (IRC) calculations [54].

4. Results and discussion

4.1. Experimental results

4.1.1. Protonated 3-iodotyrosine

Electrospraying a solution of 3-iodotyrosine in 1:1 (v/v) water/ethanol (Fig. 1) produced an abundance of protonated 3-iodotyrosine ions $[M+H]^+$ (*m/z* 308). Products of in-source fragmentation: ions at *m/z* 291, resulting from the loss of NH_3, and at *m/z* 262, the concomitant loss of H_2O and CO, from protonated 3-iodotyrosine were also evident.

The CID spectrum of protonated 3-iodotyrosine is shown in Fig. 2 and energy breakdown curves are given in Fig. 3. Unambiguous assignment of the peaks was made by comparing the product ion spectra of protonated 3-iodotyrosine, $[M+H]^+$ (Fig. 2a) and deuterated d_5-3-iodotyrosine $[M^*+D]^+$ (3-iodo-L-tyrosine with its NH_2, COOH and OH hydrogen atoms replaced by deuterium atoms, and complexed to a deuterium ion, for a total of one positive charge, Fig. 2b). A comparison between Fig. 2a and b provides information on the number of labile (exchangeable) hydrogen atoms contained within the product ions. From this comparison, it is apparent that in Fig. 2b the ion at *m/z* 274 contains one exchangeable hydrogen; those at *m/z* 96, 166, 251, 275 and 293 contain two exchangeable hydrogen atoms; those at *m/z* 97, 138, 167, 252, 265 and 294 three exchangeable hydrogen atoms; and, finally, those at 139, 168, 266 and 295 four exchangeable hydrogen atoms.

The energy breakdown curves (Fig. 3) show that, at low collision energies, the loss of NH_3 is competitive with the concomitant loss of H_2O and CO but, unlike in the CID of protonated tyrosine [30,37], the loss of NH_3 is never the dominant channel. Introduction of the electron-withdrawing iodo-substituent into the phenyl ring has made the phenyl ring less nucleophilic and raised the barrier against the loss of NH_3.

The fragmentation pattern of protonated 3-iodotyrosine $[M+H]^+$ due to resonant excitation obtained using the ion trap is qualitatively identical to the pattern shown in Fig. 2a. These ions were further isolated and allowed to fragment in order to obtain several MS^n spectra ($n \leq 5$). Representative samples of these spectra are shown in Figs. 4 and 5. The ion lineage data obtained from these experiments are summarized in Fig. 6, along with data for the fragmentation of the other ions (including protonated tyrosine [30]). Fig. 3 shows that protonated 3-iodotyrosine $[M+H]^+$ initially fragments to form two species at *m/z* 262 and 291. The precursor ion spectrum of the ion at *m/z* 291 shows that $[M+H]^+$ (*m/z* 308) is the major source of this ion. This ion is also seen in the CID spectrum of $[M+H]^+$ (Fig. 2a); the corresponding ions in the deuterated analogue $[M^*+D]^+$ are observed at *m/z* 293, 294 and 295 (Fig. 2b) and are attributed to losses of ND_3, ND_2H and NDH_2, respectively, from $[M^*+D]^+$. These observations serve to substantiate the assignment of this ion (*m/z* 291 in Fig. 1) as being $[M+H-NH_3]^+$.

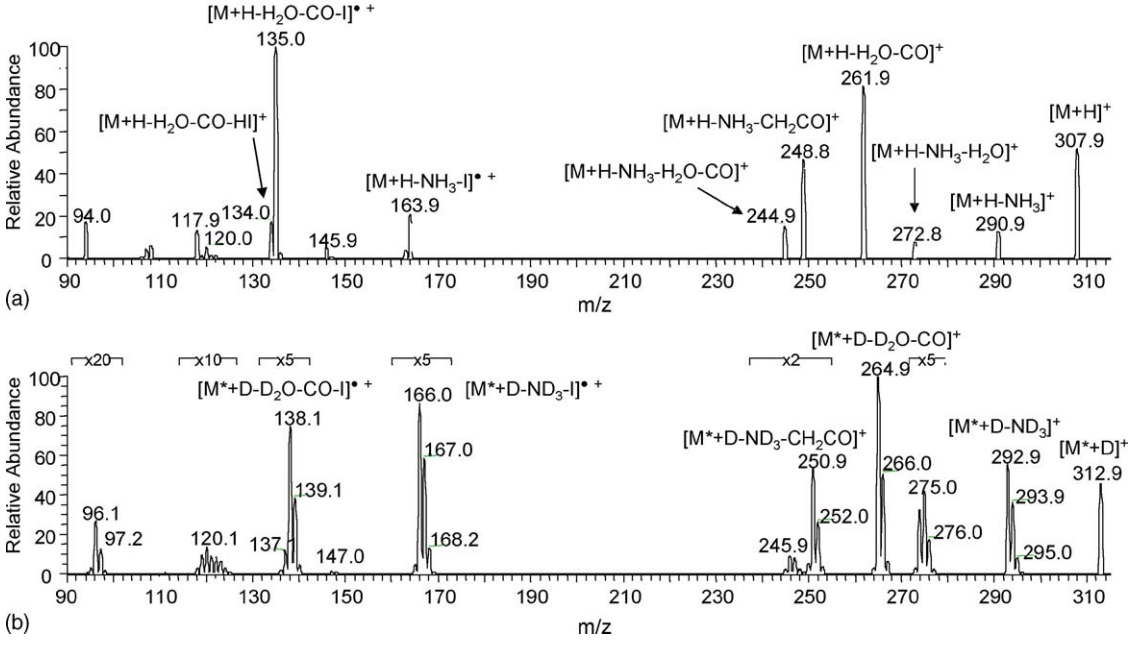

Fig. 2. CID of 3-iodotyrosine (a) in H_2O/CH_3OH solution, $[M+H]^+$ and (b) in D_2O/CH_3OD solution, $[M^*+D]^+$ obtained on the LCQ ion trap.

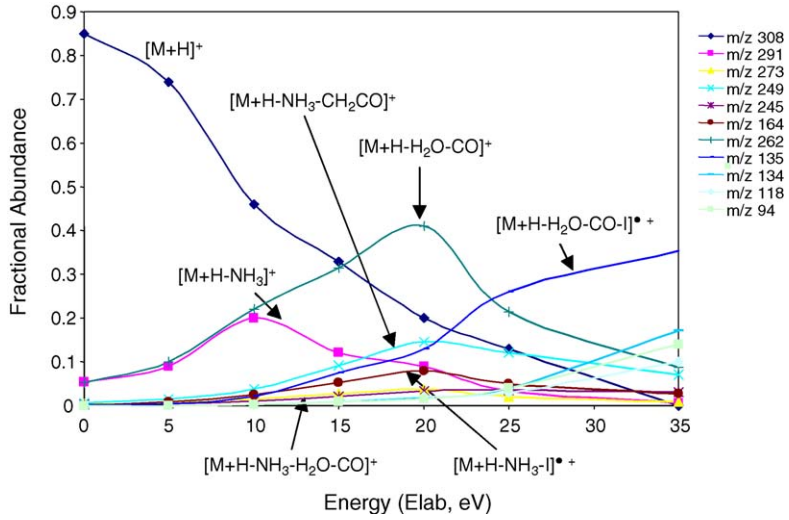

Fig. 3. Energy breakdown curves for the CID of protonated 3-iodotyrosine obtained on the LCQ ion trap.

The $[M+H-NH_3]^+$ ion (*m/z* 291 Figs. 1 and 2a) further fragments to generate five ions at *m/z* 273, 249, 245, 164 and 146 (Figs. 4a and 6). Four of these ions and their subsequent fragments are examined here in detail while the ion at *m/z* 146, which represented a very minor species, will not be discussed further. The ion at *m/z* 273 was assigned as $[M+H-NH_3-H_2O]^+$ (Fig. 4a). The precursor ion spectrum of this species shows ions $[M+H-NH_3]^+$ (*m/z* 291) and $[M+H]^+$ (*m/z* 308) as its sources, which validates its assignment to be due to the loss of water from $[M+H-NH_3]^+$ (*m/z* 291). The ions observed for the deuterated analogue at *m/z* 274, 275, 276 (Fig. 2b) indicate the extent of gas-phase H/D scrambling that occurs prior to the consecutive losses of NH_3 and H_2O from $[M+H]^+$. The subsequent loss of CO from $[M+H-NH_3-H_2O]^+$ (*m/z* 273 in Figs. 2a, 4a and 5) produces an ion at *m/z* 245 which in turn loses a neutral fragment of 127 Da, most likely $I^\bullet$, to generate a radical cation at *m/z* 118. The precursor ion spectra of the species at *m/z* 245 and *m/z* 118 clearly show the ions at *m/z* 273 and *m/z* 245 to be major sources for their respective formation.

The $[M+H-NH_3]^+$ ion also dissociates to produce an ion at *m/z* 249 assigned as $[M+H-NH_3-CH_2CO]^+$ (Figs. 2a, 4a and 5). The precursor ion spectrum of *m/z* 249 shows the major sources of these ions to be $[M+H-NH_3]^+$ (*m/z* 291) and $[M+H]^+$ (*m/z* 308). The ion at *m/z* 249 is thus most likely due to the loss of ketene, CH_2CO, from $[M+H-NH_3]^+$. This is also consistent with the ions at *m/z* 251 and 252 (Fig. 2b) observed due to the loss of CH_2CO from, respectively $[M+H-ND_3]^+$ and $[M+H-ND_2H]^+$. Furthermore, the relative abundances of ions at *m/z* 292 and 293 are similar to those at *m/z* 251 and 252, indicating that the neutral lost does not carry a D atom.

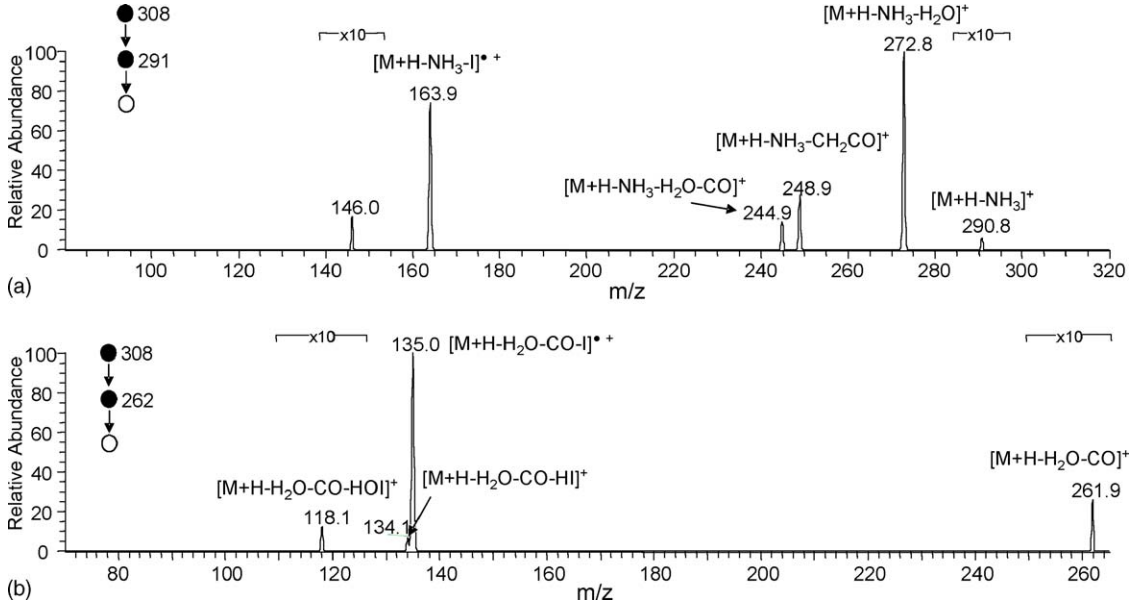

Fig. 4. Tandem mass spectra (a) of the fragment ion at *m/z* 291 and (b) of the fragment ion at *m/z* 262; both generated on the LCQ ion trap from protonated 3-iodotyrosine.

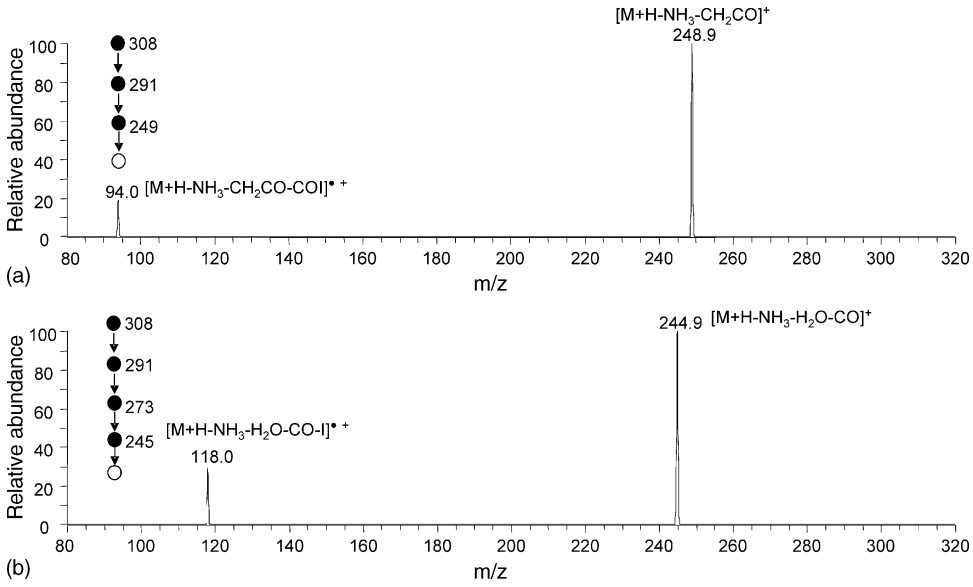

Fig. 5. Tandem mass spectra (a) of the fragment ion at *m/z* 249 and (b) of the fragment ion at *m/z* 245; both generated on the LCQ ion trap from protonated 3-iodotyrosine.

The low abundance of the ion at *m/z* 253 is then a result of the low abundance of the ion $[M+H-NDH_2]^+$ at *m/z* 295 (Fig. 2b). The $[M+H-NH_3-CH_2CO]^+$ ion is probably protonated 3-iodo-4-hydroxybenzaldehyde. This ion can further dissociate to produce an ion at *m/z* 94 (Figs. 2a and 5a and the precursor ion spectrum of *m/z* 94), a fragmentation that probably involves the losses of I• (127 Da) and CO (28 Da). The most plausible product is the radical cation of phenol, but formation of this ion requires migration of two hydrogen atoms.

The ion at *m/z* 245 (Figs. 2a and 4a), produced in the fragmentation of $[M+H-NH_3]^+$ (*m/z* 291 Fig. 4a), is most likely

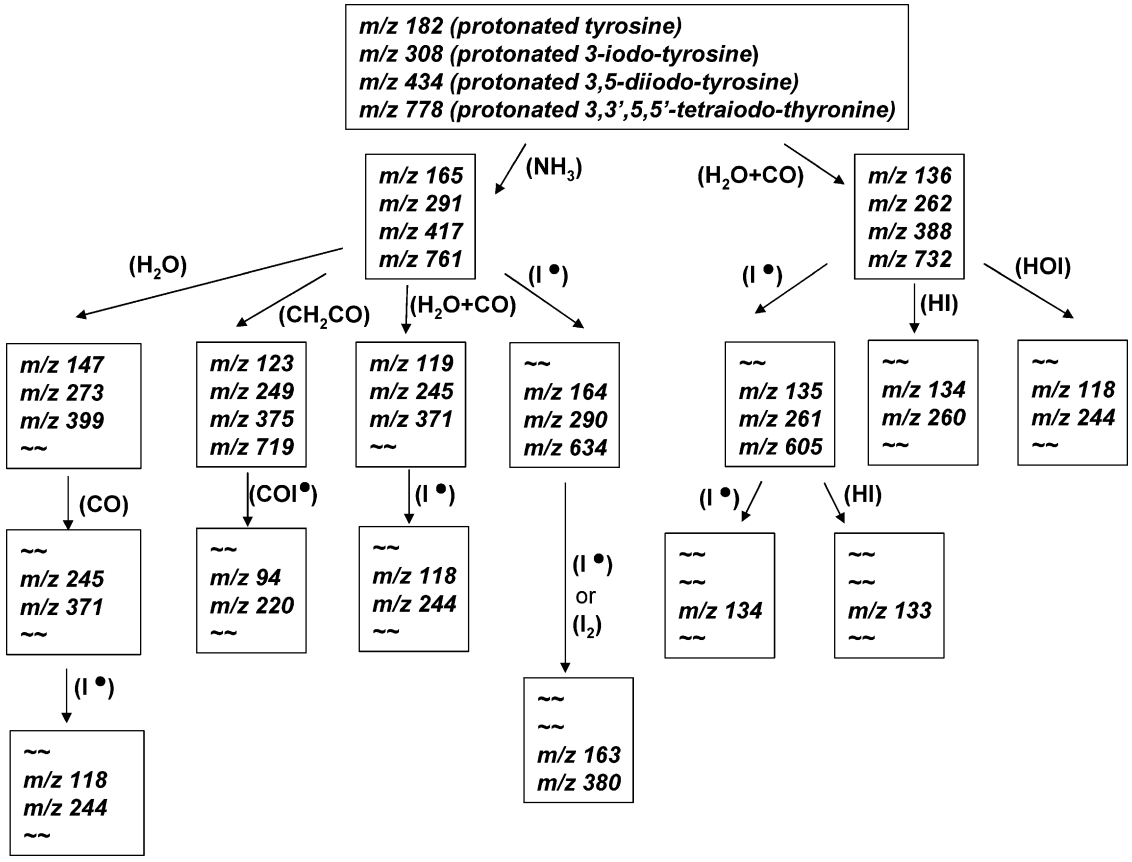

Fig. 6. Fragmentation pathways of protonated tyrosine and iodotyrosines.

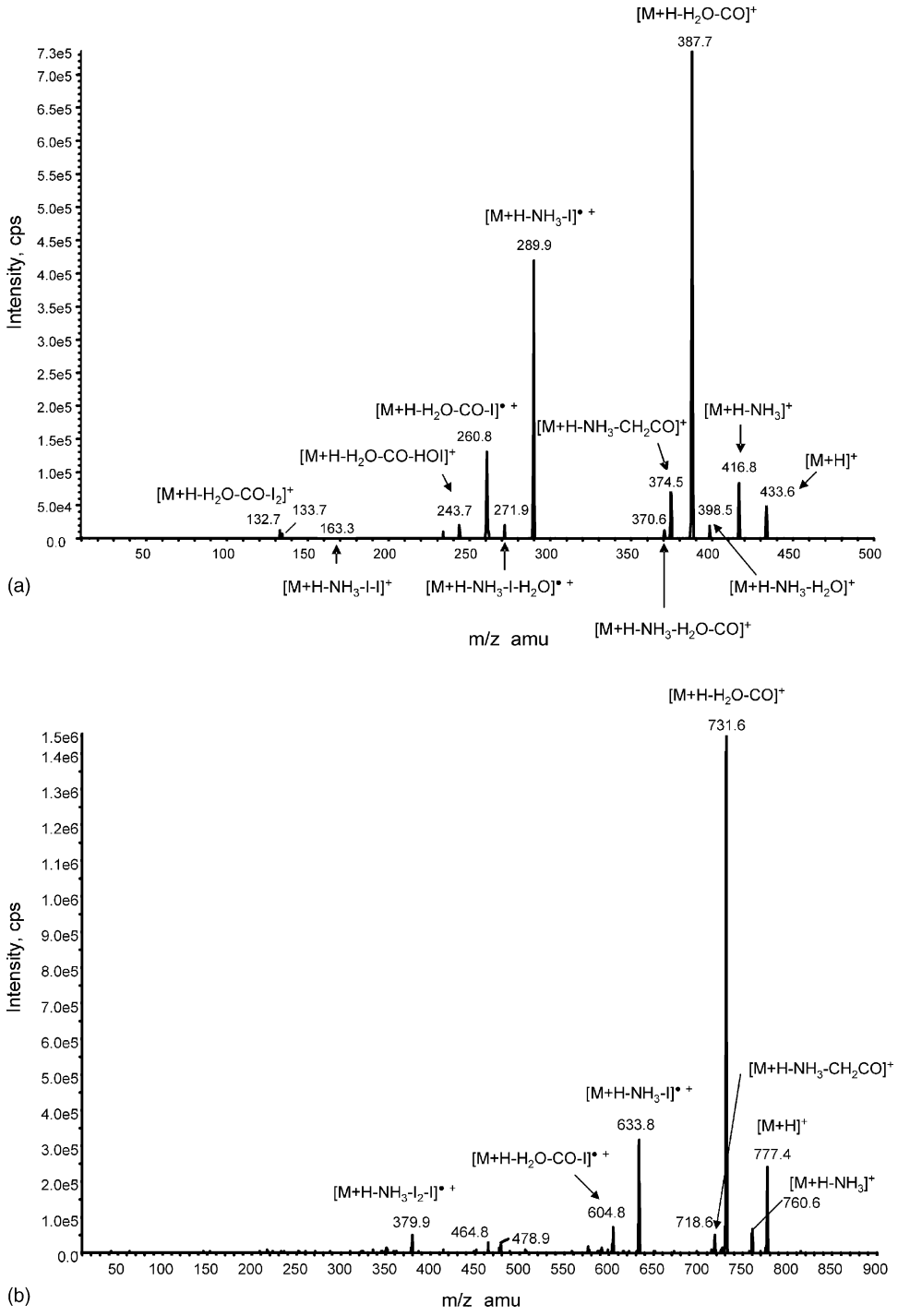

Fig. 7. CID spectra of (a) protonated 3,5-diiodotyrosine at $E_{lab} = 30$ eV and (b) protonated thyroxine at $E_{lab} = 35$ eV (both obtained on the API 3000).

due to the concomitant loss of H_2O and CO. The precursor ion spectrum for $[M+H-NH_3-H_2O-CO]^+$ shows four ions as possible sources. These are $[M+H]^+$ (m/z 308), $[M+H-NH_3]^+$ (m/z 291), $[M+H-NH_3-H_2O]^+$ (m/z 273) and an ion at m/z 262, that may correspond to $[M+H-H_2O-CO]^+$. The ion-trap-generated MS^3 spectrum shown in Fig. 4a can account for the first three ions as a source of a cationic species at m/z 245. There is, however, no m/z 245 ion in the MS^3 spectrum of $[M+H-H_2O-CO]^+$ (Fig. 4b). This suggests that the species at m/z 262 observed in the precursor ion spectrum is not $[M+H-H_2O-CO]^+$, but rather an isobaric ion present in the solution that fortuitously fragments to produce a species at m/z 245.

The MS^3 spectrum of $[M+H-NH_3]^+$ (m/z 291 Fig. 4a) shows a product ion at m/z 164 (Figs. 2a and 4a), corresponding to the loss of $I^\bullet$. The precursor ion scan shows $[M+H-NH_3]^+$

and $[M+H]^+$ to generate this ion. Fig. 4b shows three ions at *m/z* 166, 167 and 168 corresponding to the loss of $I^\bullet$ from each of $[M^* + D - ND_3]^+$, $[M^* + D - ND_2H]^+$ and $[M^* + D - NDH_2]^+$, respectively.

Electrospraying a solution of 3-iodotyrosine (Fig. 1) produced an ion at *m/z* 262 which was assigned the structure of the iminium ion (analogous to the a_1 ion from peptide fragmentation) formed by the concomitant loss of H_2O and CO via in-source fragmentation of the $[M+H]^+$ ion. The precursor ion spectrum of the ion at *m/z* 262 shows the only source of these ions to be the $[M+H]^+$ ion at *m/z* 308, while the ions at *m/z* 265, 266 (Fig. 2b) are consistent with the formation of this iminium ion via the concomitant losses of, respectively, D_2O plus CO, and HOD plus CO from $[M^* + D]^+$.

CID of the iminium ion $[M+H-H_2O-CO]^+$ (*m/z* 262 in Fig. 4b) produces three fragment ions at *m/z* 135, 134 and 118, with the latter two being minor species. The major ion at *m/z* 135 is most likely due to the loss of $I^\bullet$, while the minor species at *m/z* 134 and 118 are likely due to losses of, respectively, HI and HOI.

4.1.2. Protonated 3,5-diiodotyrosine

The spectrum of protonated 3,5-diiodotyrosine (*m/z* 434) exhibits several fragmentation pathways (Figs. 7a and 8a) that are identical to those of protonated 3-iodotyrosine; these include the elimination of NH_3 to form the ion at *m/z* 417 and the concomitant loss of H_2O and CO to form the ion at *m/z* 388. From the energy breakdown curves (Fig. 8a), it is apparent that the threshold for eliminating H_2O and CO is lower than that for eliminating NH_3. This is different from the CID of protonated tyrosine and 3-iodotyrosine. We interpret this difference as a consequence of the additional electron-withdrawing effect from the second iodo-substituent on the phenyl ring.

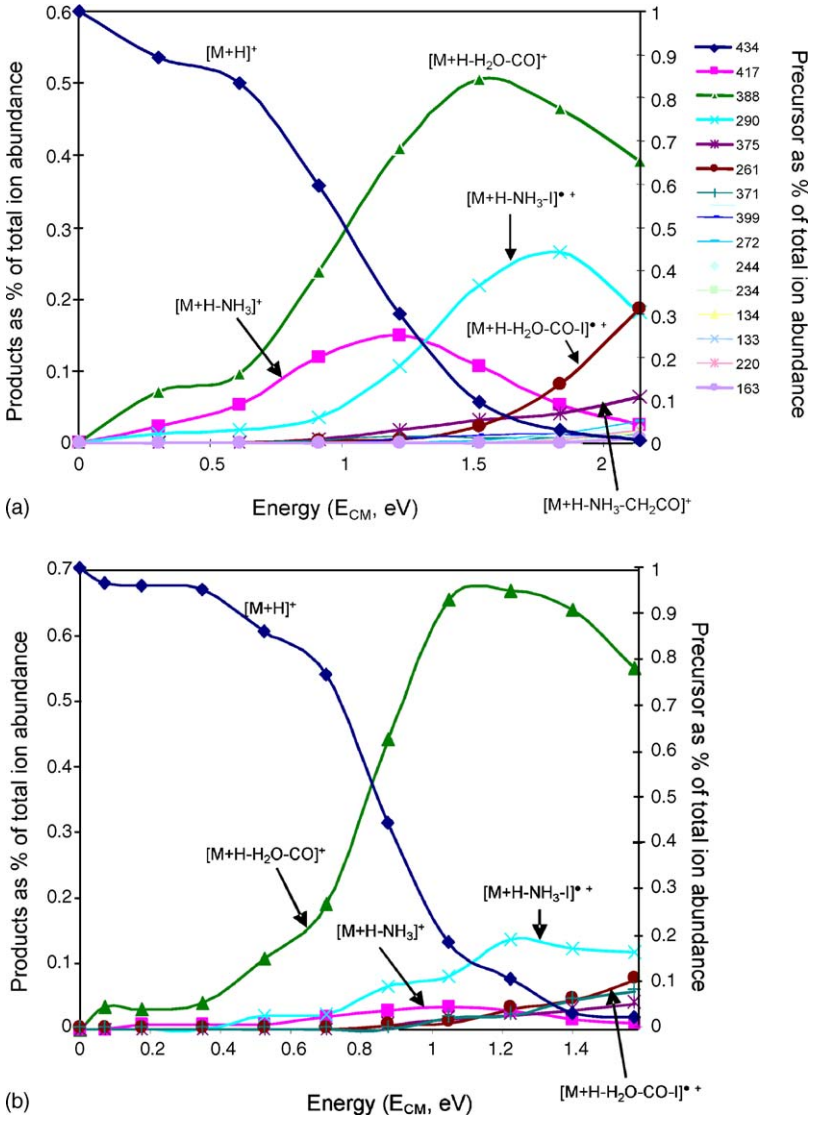

Fig. 8. Energy breakdown curves for (a) protonated 3,5-diiodotyrosine and (b) protonated thyroxine obtained on the API 3000.

Inspection of Fig. 6 shows the similarities in the CID products of protonated 3,5-diodotyrosine and protonated 3-iodotyrosine, but there are differences in relative abundances. The dominant pathway in the fragmentation of ion $[M+H-NH_3]^+$ from protonated diiodotyrosine is loss of $I^\bullet$ to give the ion at *m/z* 290; the loss of ketene to give the ion at *m/z* 375 is a minor channel (Figs. 7a and 8a). Both pathways are present in the CID of protonated 3-iodotyrosine, but here the loss of ketene is dominant.

All other pathways observed in the CID of protonated 3-iodotyrosine also exist in that of protonated 3,5-diiodotyrosine; however, the only significant product, other than those already discussed, is the ion at *m/z* 261, formed by eliminating $I^\bullet$ from the iminium ion, $[M+H-H_2O-CO]^+$. The iminium ion also loses HI and HOI, giving ions at, respectively, *m/z* 260 and 244, but these products are in very low abundances. At high collision energies, ions at *m/z* 134 and 133, corresponding to loss of the second iodine atom, were observed.

4.1.3. Protonated thyroxine

The concomitant loss of H_2O and CO is the dominant fragmentation pathway at all collision energies (Figs. 7b and 8b), giving an ion at *m/z* 732 to which we assign the iminium ion structure. The loss of NH_3 from protonated thyroxine is also observed, but the product ion (*m/z* 761) is in very low abundance and appears to easily lose $I^\bullet$ to give an ion at *m/z* 634. As in the CID of the $[M+H-NH_3]^+$ ions generated from the other protonated tyrosines, the loss of ketene occurs, but the product ion is much lower in abundance than that from the loss of $I^\bullet$.

An ion at *m/z* 380 was observed at higher collision energies and this is attributed to $[M+H-NH_3-I^\bullet-I_2]^+$. Curiously, the ion at *m/z* 507, corresponding to the loss of only two iodine atoms, was observed in much lower abundance (Fig. 7b).

4.2. Theoretical studies on the fragmentation mechanisms of protonated 3-iodo-tyrosine

4.2.1. Concomitant loss of H_2O and CO and subsequent reactions on pathway 1

The preferred site of protonation on tyrosines is the α-amino nitrogen atom, with one proton from the NH_3^+ group hydrogen-bonding to the carbonyl oxygen and another interacting with the π-cloud over the ipso-carbon of the phenyl ring (structure **1**, Fig. 9). The rate-determining barrier against the concomitant loss of H_2O and CO from protonated substituted tyrosines has been shown to be the transfer of a proton from the NH_3^+ group to the OH of the COOH [37,39,41]. This barrier is almost independent of the electron-donating ability of the substituent in the phenyl ring (ranging from 37.8 kcal/mol for *p*-NO_2 to 39.2 kcal/mol for *p*-NH_2 [37]). For 3-iodotyrosine, the overall endothermicity, ΔH_0°, as calculated at B3LYP/DZVP for the loss of H_2O and CO, is 29.8 kcal/mol (Fig. 9); this compares with values in the range 22.9–25.8 kcal/mol calculated at B3LYP/6-31G(d,p) [37].

The breakdown curves (Fig. 3) indicated that the iminium ion $[M+H-H_2O-CO]^+$ is quite stable towards CID. The dominant pathway in its decomposition is the loss of $I^\bullet$, with losses of HI and HOI being much less common. Fig. 9 gives the structures of the ions produced by these three pathways (ions **3**–**5**), and the ΔH_0° and ΔG_{298}° for their formation, relative to protonated 3-iodotyrosine. In terms of endothermicities, the ΔH_0°

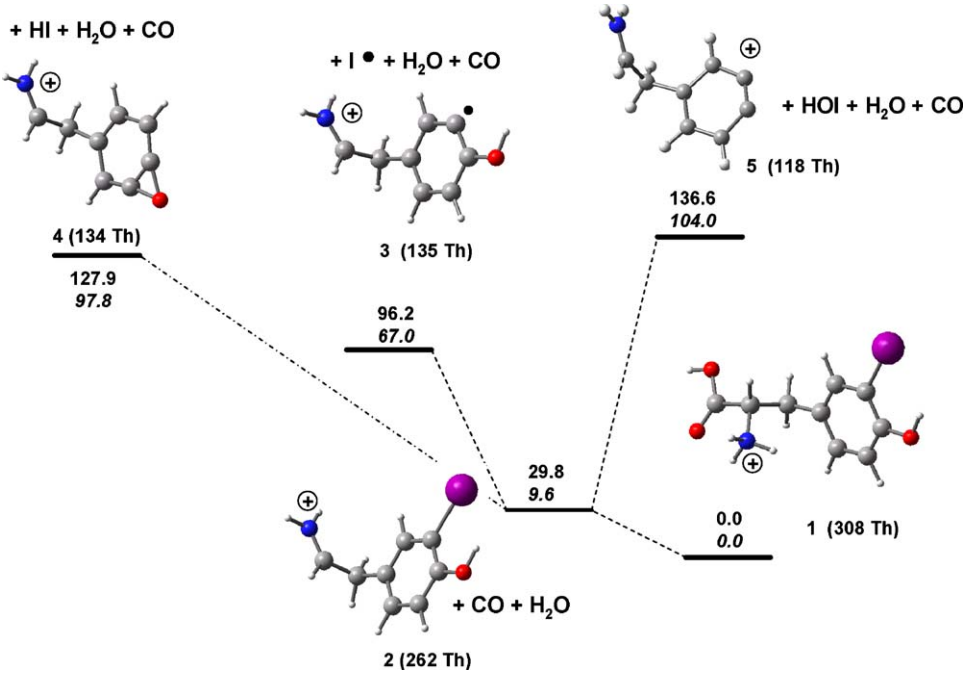

Fig. 9. Energy profile for the concomitant loss of H_2O plus CO and beyond from protonated 3-iodotyrosine. Upper numbers are enthalpies at 0 K and lower italicized numbers are free energies at 298 K (both in kcal/mol).

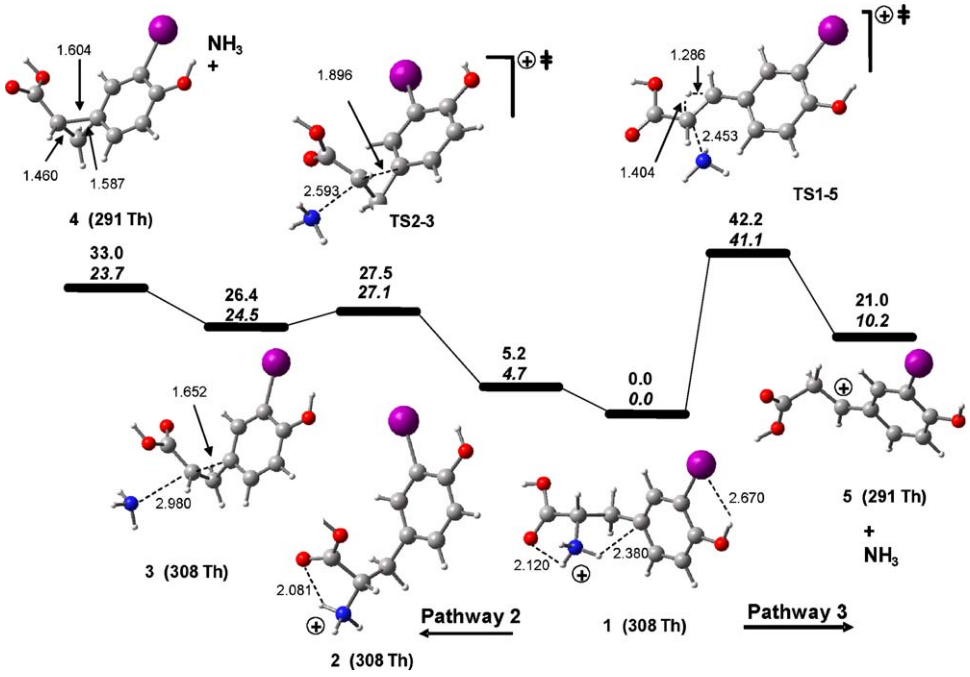

Fig. 10. Energy profile for the loss of NH_3 via pathways 2 and 3 from protonated 3-iodotyrosine. Upper numbers are enthalpies at 0 K and lower italicized numbers are free energies at 298 K (both in kcal/mol).

values are $I^{\bullet}$ loss < HI loss < HOI loss, consistent with the experimental observation.

4.2.2. Loss of ammonia and subsequent fragmentations on pathway 2

As reported previously, loss of ammonia from protonated tyrosine can occur by one of two mechanisms, internal displacement by the aryl group (the neighboring-group mechanism) forming a phenonium ion, or displacement by a hydride ion from the CH_2 forming a benzyl cation. For protonated tyrosine, the barriers against these processes are calculated to be 26.5 and 40.8 kcal/mol, respectively [37]. Introduction of an iodo-substituent *ortho* to the hydroxy group diminishes the ability of the phenyl ring to stabilize a positive charge and destabilizes both the phenonium ion and the benzyl cation. The barriers against deamination of protonated 3-iodotyrosine by these two mechanisms, as calculated at B3LYP/DZVP (shown in Fig. 10), are 33.0 (the endothermicity of the reaction) and 42.2 kcal/mol (taken from the energy of the transition state for the synchronous loss of NH_3 and hydride migration), respectively. Both barriers are higher than the values reported for protonated tyrosine, with the larger destabilizing effect being for formation of the phenonium ion (6.5 compared with 1.4 kcal/mol). Assuming that the barrier against the concomitant loss of H_2O and CO is in the range 37–39 kcal/mol [37], then the loss of NH_3 via the phenonium ion mechanism should be the dominant channel at very low collision energies. From Fig. 3, both appear to have similar energies. Here we note that for protonated 4-nitrophenylalanine the calculated barriers against the loss of NH_3 and the concomitant loss of H_2O and CO are very close (38.7 and 37.8 kcal/mol, respectively [37]), but the only product observed was from the loss of H_2O and CO. If introduction of a second iodo-substituent raises the barrier against NH_3 loss by a similar amount as the first one, then the barriers for the two pathways will be almost identical. It is evident from Fig. 8a that both pathways are observed at low collision energies; at higher collision energies, the loss of $I^{\bullet}$ occurs subsequent to that of NH_3.

The phenonium ions have limited stability in the gas phase. Conversion of phenonium ion **8** into benzyl cation **9** involves a single-step process in which the long C–C bond of the 3-membered ring is broken accompanied by a 1,2-hydride shift. We calculate the enthalpy of activation for this rearrangement to be 25.8 kcal/mol. From the energy breakdown curves (Fig. 3), the lowest-energy fragmentation pathway for ion $[M+H-NH_3]^+$ is the loss of ketene. Mechanistically, this is difficult to achieve from the phenonium ion and we propose that initially rearrangement to the thermodynamically more stable benzyl cation occurs, followed by a 1,3-OH migration from the carboxy group to the exocyclic carbon that formally carries the positive charge (Fig. 11a) [30]. The barrier against the loss of ketene from the intermediate acylium ion, **10**, is almost identical to that for its formation; the overall $\Delta H_0^{\circ\ddagger}$ and $\Delta G_{298}^{\circ\ddagger}$ values of 53.4 and 42.7 kcal/mol for the loss of ketene are much lower than those for fragmentation of the iminium ion (Fig. 9). The product ion, protonated 3-iodo-4-hydroxybenzaldehyde, **11**, loses CO and $I^{\bullet}$ to give an ion at *m/z* 94 (Fig. 5a) to which we have assigned the phenol radical cation structure, **12**. This is the only product ion observed in the CID of ion **11** and the calculated of ΔH_0° and ΔG_{298}° values for the formation of **12** from **11** are 44.7 and 29.4 kcal/mol, respectively; formation of **12** requires migration of two hydrogens from the side chain, one to replace the iodine and the

other to displace the CO. We have not pursued the mechanism of this reaction due to its complexity and because the abundance of **12** is very low for collision energies less than 20 eV (Fig. 3).

Loss of a water molecule from **9** involves the OH of COOH and a hydrogen from the adjacent CH_2 and creates a solvated benzyl cation with a ketene side chain, ion **13** (Fig. 11b). The solvating water molecule in **13** is loosely bound (binding enthalpy at 0 K is 10.0 kcal/mol); under CID conditions **14** is probably formed directly from **9**. The enthalpy of activation at 0 K is 19.7 kcal/mol higher than that for the formation of ketene and hence the loss of water only becomes competitive at higher collision energies.

The subsequent loss of CO to give ion **15**, another phenonium ion, has a $\Delta H_0^{\circ\ddagger}$ of 79.2 kcal/mol relative to the benzyl cation. This isomerizes via **TS15–16** to give the thermodynamically more stable α-arylvinyl cation, **16** (Fig. 11b). On this pathway, the highest barrier at **TS15–16** is 93.3 kcal/mol above **9**. Alternatively, ion **16** can be obtained from **9** by the loss of water involving loss of the benzylic hydrogen and forming an acylium ion **19** that spontaneously loses CO to give vinyl cation **16** (Fig. 11c). The highest transition state along this pathway

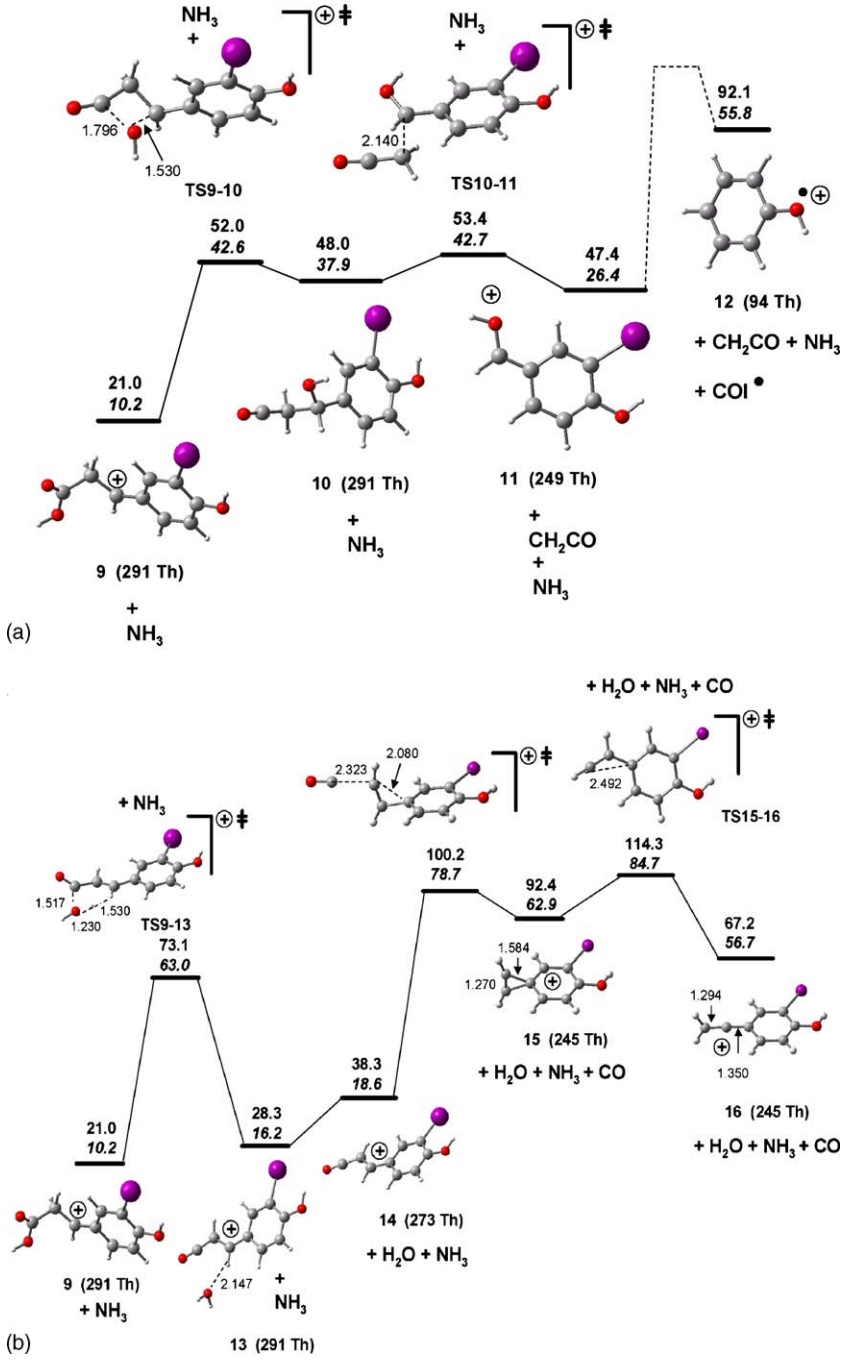

Fig. 11. Energy profiles for competitive losses from the benzyl cation generated from protonated 3-iodotyrosine. Upper numbers are enthalpies at 0 K and lower italicized numbers are free energies at 298 K (both in kcal/mol).

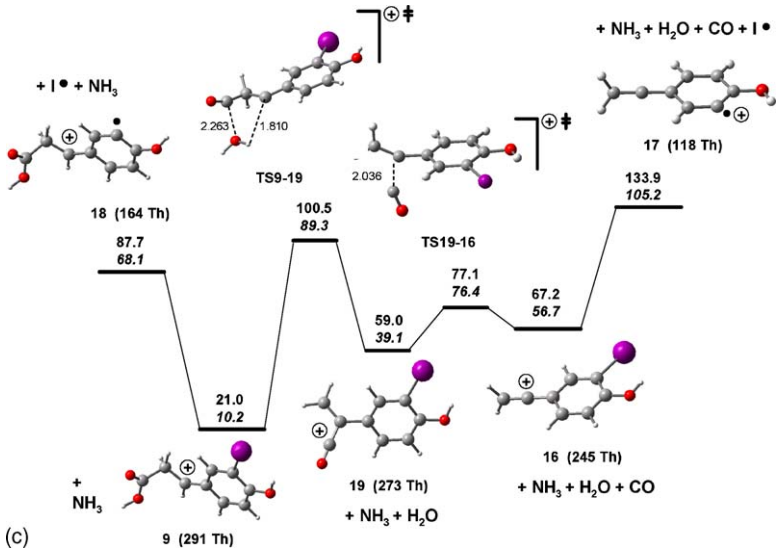

Fig. 11. (*Continued*).

has an enthalpy of activation 79.5 kcal/mol above the benzyl cation; hence this is a lower energy pathway to ion **16**. The loss of I• from the vinyl cation **16** to produce the radical cation **17** is endothermic by 66.7 kcal/mol (Fig. 11c).

Summarizing the computational results for the fragmentation of benzyl cation **9**, the enthalpies (in kcal/mol) against the following eliminations are: loss of ketene, 53.4; loss of water, 73.1; loss of iodine atom, 87.7; concomitant loss of water and carbon monoxide, 100.5.

4.2.3. Linear free energy relationships

The ease with which the loss of NH_3 occurs via the neighboring-group mechanism (pathway 2) is strongly influenced by the nucleophilicity of the aromatic ring; by comparison, the rate-determining step in the concomitant loss of H_2O and CO involves proton transfer from NH_3^+ to the OH of the COOH group, a reaction that is remote from the ring and, therefore, has little sensitivity to substituents. We optimized the transition state and product structures for the formation of the phenonium ions from protonated tyrosine, from derivatives that have iodo-substituents *ortho* to the OH group and from protonated 3,5-diiodo,4-phenoxytyrosine. There are many structural similarities between these structures but the energies are sensitive to the substituents (Cartesian coordinates and electronic energies for key structures are available as Supporting Information). For each ion, the transition state is lower in energy than the products (Table 1). The $\Delta H_0^{\circ\ddagger}$ and $\Delta G_{298}^{\circ\ddagger}$ are similar, but ΔG_{298}° for the overall reaction are considerably smaller than ΔH_0°, reflecting the formation of two molecules from one. Plots of $\Delta H_0^{\circ\ddagger}$ and

Table 1
Calculated enthalpies and free energies of the transition states and the separated products for the formation of the phenonium ions at B3LYP/DZVP level, relative to the lowest energy conformers of protonated tyrosine and iodotyrosines

Derivatives	σ_x^{+}[a]	TS energy (kcal/mol)		Products (kcal/mol)	
		$\Delta H_0^{\circ\ddagger}$	$\Delta G_{298}^{\circ\ddagger}$	$\Delta H_0^{\circ R}$	$\Delta G_{298}^{\circ R}$
1 R_3 = H, R_4 = OH	−0.92	26.8	26.3	31.9	22.5
2 R_3 = I, R_4 = OH	−0.57	27.5	27.1	33.0	23.7
3 R_3 = I, R_4 = OH, R_5 = I	−0.22	28.8	28.3	34.7	25.4
4 R_3 = I, R_4 = OPh, R_5 = I	0.20	31.1	31.0	36.7	28.0

[a] The substituent constants are from Ref. [46].

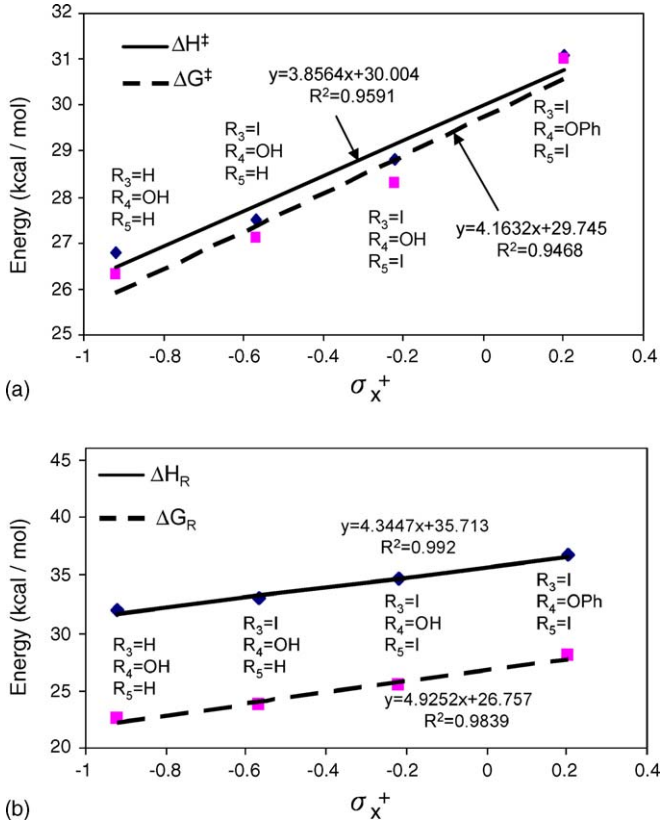

Fig. 12. Plots of (a) activation energies and (b) endothermicities of the reactions (both in kcal/mol) for NH_3 loss from protonated substituted tyrosine derivatives via the neighboring-group displacement mechanism (pathway 2) versus σ_x^{+}.

$\Delta G^{\circ}_{298}{}^{\ddagger}$ versus σ^+ both give straight lines with correlation coefficients of 0.96 and 0.95, respectively (Fig. 12a). Plots of ΔH°_0 and ΔG°_{298} for the overall reaction are more important, as they provide the barriers against the loss of NH_3 by the neighboring-group mechanism. Plots of these calculated values versus σ^+ show even better correlations with correlation coefficients of 0.99 and 0.98, respectively (Fig. 12b).

5. Conclusions

In collision-induced dissociation, protonated tyrosine fragments by the loss of NH_3 via pathway 2; a second channel, the concomitant loss of H_2O and CO (pathway 1), is relatively minor. Introduction of electron-withdrawing groups, specifically iodines, into the 3- and/or 5-positions of the phenyl ring, results in pathway 1 becoming increasingly more important. Pathway 1 is even more dominant in the CID spectrum of protonated thyroxine, in which there are two iodo-substituents in the phenyl ring and the *p*-OH of tyrosine has been converted into a 3,5-diiodo-4-hydroxyphenoxy group.

The relative abundances of ions resulting from either the loss of NH_3 or the concomitant loss of H_2O and CO are easily understood in terms of the effect of substituents on the two competing pathways. For pathway 1, a previous study has shown that the rate-determining step is proton transfer from the $NH_3{}^+$ of the protonated amino acid to the OH of the COOH group. Both these groups are not conjugated with the phenyl ring. This remoteness of the reaction centers from the substituents results in a very small variation in the barrier against the concomitant loss of H_2O and CO, as the substituents are varied. By contrast, the loss of NH_3 by pathway 2 (and also by the higher-energy pathway 3) is heavily dependent on the substituents. The *p*-OH group is strongly π-donating, the *p*-OPh group a weaker π-donor, and *m*-iodo weakly electron-withdrawing. Rates for electrophilic substitution have previously been shown to correlate well with σ^+ values; for pathway 2, where the nucleophilicity of the phenyl group decreases from that in tyrosine to that in 3,5-diiodo-4-phenoxytyrosine, we find a similar type of dependence. We conclude, therefore, that it is the electron-donating ability of the substituents in the phenyl ring that determines whether the loss of NH_3 or the concomitant loss of H_2O and CO is the dominant channel at low collision energies.

Ions $[M+H-NH_3]^+$ fragment by two competing pathways, loss of ketene via a reaction involving 1,3-migration of OH from the carboxylic group to the cationic carbon of the benzyl cation, and loss of $I^{\bullet}$. For protonated 3-iodotyrosine loss of ketene is the dominant channel, while for the more heavily iodinated ions loss of $I^{\bullet}$ is preferred. The iminium ions, $[M+H-H_2O-CO]^+$, are more stable towards collision-induced dissociation, but at higher collisional energies the dominant pathways in their dissociations is loss of $I^{\bullet}$. Density functional calculations support these observations. Loss of $I^{\bullet}$ from iminium ion **2** is calculated to be endothermic by 96.2 kcal/mol (relative to the starting structure of protonated 3-iodotyrosine) while loss of ketene from the benzyl cation, **9**, formed via the intermediacy of phenonium ion **8**, is 58 kcal/mol.

Acknowledgments

This work was supported by the Natural Sciences and Engineering Research Council (NSERC) of Canada, MDS SCIEX and York University. T.S. wishes to thank Dr. Zoltan Mester at the Institute for National Measurement Standards in whose laboratory some of this research was performed.

Appendix A. Supplementary data

Supplementary data associated with this article can be found, in the online version, at doi:10.1016/j.ijms.2006.03.012.

References

[1] J.B. Fenn, M. Mann, C.K. Meng, S.F. Wong, C.M. Wong, Science 246 (1989) 64.
[2] M. Karas, F. Hillenkamp, Anal. Chem. 60 (1988) 2299.
[3] R. Aebersold, D.R. Goodlett, Chem. Rev. 101 (2001) 269.
[4] D.F. Hunt, J.R. Yates, J. Shababnonowitz, S. Winston, C.R. Hauer, Proc. Natl. Acad. Sci. U.S.A. 83 (1986) 6233.
[5] R.S. Johnson, S.A. Martin, K. Biemann, Int. J. Mass Spectrom. 86 (1988) 137.
[6] M. Mann, P. Hojrup, P. Roepstorff, Biol. Mass Spectrom. 22 (1993) 338.
[7] J.K. Eng, A.L. McCormack, J.R. Yates, J. Am. Soc. Mass Spectrom. 5 (1994) 976.
[8] X. Tang, P. Thibault, R.K. Boyd, Anal. Chem. 65 (1993) 2824.
[9] J.A. Taylor, R.S. Johnson, Anal. Chem. 73 (2001) 2594.
[10] M.M. Cordero, J.J. Houser, C. Wesdemiotis, Anal. Chem. 65 (1993) 1594.
[11] K. Ambihapathy, T. Yalcin, H.W. Leung, A.G. Harrison, J. Mass Spectrom. 32 (1997) 209.
[12] A.G. Harrison, I.G. Csizmadia, T.H. Tang, Y.P. Tu, J. Mass Spectrom. 35 (2000) 683.
[13] A.G. Harrison, Int. J. Mass Spectrom. 217 (2002) 185.
[14] A.G. Harrison, J. Mass Spectrom. 38 (2003) 174.
[15] M.J. Nold, C. Wesdemiotis, T. Yalcin, A.G. Harrison, Int. J. Mass Spectrom. 164 (1997) 137.
[16] J.M. Farrugia, T. Taverner, R.A.J. O'Hair, Int. J. Mass Spectrom. 209 (2001) 99.
[17] R.A.J. O'Hair, J. Mass Spectrom. 35 (2000) 1377.
[18] B. Paisz, S. Suhai, Mass Spec. Rev. 24 (2005) 508.
[19] T. Yalcin, C. Khouw, I.G. Csizmadia, M.R. Peterson, A.G. Harrison, J. Am. Soc. Mass Spectrom. 6 (1995) 1164.
[20] T. Yalcin, I.G. Csizmadia, M.R. Peterson, A.G. Harrison, J. Am. Soc. Mass Spectrom. 7 (1996) 233.
[21] R.A.J. O'Hair, G.E. Reid, Eur. Mass Spectrom. 5 (1999) 325.
[22] C.F. Rodriquez, A. Cunje, T. Shoeib, A.C. Hopkinson, K.W.M. Siu, J. Am. Chem. Soc. 123 (2001) 3006.
[23] B. Paizs, S. Suhai, Rapid Commun. Mass Spectrom. 15 (2001) 2307.
[24] B. Paizs, S. Suhai, Rapid Commun. Mass Spectrom. 16 (2002) 375.
[25] H. El Aribi, C.F. Rodriquez, D.R.P. Almeida, Y. Ling, W.W.N. Mak, A.C. Hopkinson, K.W.M. Siu, J. Am. Chem. Soc. 125 (2003) 9229.
[26] B. Paizs, S. Suhai, A.G. Harrison, J. Am. Mass Spectrom. 14 (2003) 1454.
[27] N.N. Dookeran, T. Yalcin, A.G. Harrison, J. Mass Spectrom. 31 (1996) 500.
[28] T. Yalcin, A.G. Harrison, J. Mass Spectrom. 31 (1996) 1237.
[29] F. Rogalewicz, Y. Hoppilliard, G. Ohanessian, Int. J. Mass Spectrom. 195/196 (2000) 565.
[30] H. El Aribi, G. Orlova, A.C. Hopkinson, K.W.M. Siu, J. Phys. Chem. A 108 (2004) 3844.
[31] R.A.J. O'Hair, M.L. Styles, G.E. Reid, J. Am. Soc. Mass Spectrom. 9 (1998) 1275.

[32] H. Lioe, R.A.J. O'Hair, G.E. Reid, J. Am. Soc. Mass Spectrom. 15 (2004) 65.
[33] I.P. Csonka, B. Paizs, S. Suhai, J. Mass Spectrom. 39 (2004) 1025.
[34] I. Shek, J. Zhao, Y. Ke, K.W.M. Siu, A.C. Hopkinson, J. Phys. Chem. A, in press.
[35] Z.B. Maksik, B. Kovacevic, Chem. Phys. Lett. 307 (1999) 497–504.
[36] T. Shoeib, A. Cunje, A.C. Hopkinson, K.W.M. Siu, J. Am. Soc. Mass Spectrom. 13 (2002) 408.
[37] H. Lioe, R.A.J. O'Hair, Org. Biomol. Chem. 3 (2005) 3618.
[38] E. Uggerud, Theor. Chim. Acta 97 (1997) 313.
[39] F. Rogalewicz, Y. Hoppilliard, G. Ohanessian, Int. J. Mass Spectrom. 195/196 (2000) 565.
[40] F. Rogalewicz, Y. Hoppilliard, Int. J. Mass Spectrom. 199 (2000) 235.
[41] R.A.J. O'Hair, P.S. Broughton, M.L. Styles, B.T. Frink, C.M. Hadad, J. Am. Soc. Mass Spectrom. 11 (2000) 687.
[42] B. Balta, M. Basma, V. Aviyente, Z. Chuanbao, C. Lifshitz, Int. J. Mass Spectrom. 201 (2000) 69.
[43] H.C. Brown, Y. Okamoto, J. Am. Chem. Soc. 80 (1958) 4979.
[44] A.M. Couldwell, M.C. Thomas, T.W. Mitchell, A.J. Hulbert, S.J. Blanksby, Rapid Commun. Mass Spectrom. 19 (2005) 2295.
[45] E. Dreschel, Z. Biol. 33 (1896) 85.
[46] S. Hunt, in: F. Wold, K. Moldave (Eds.), Methods of Enzymology: Post-translational Modifications (Part B), Academic Press, New York, 1984, p. 413 (Chapter 27).
[47] C. Hansch, A. Leo, R.W. Taft, Chem. Rev. 91 (1991) 165.
[48] A.D. Becke, Phys. Rev. A 38 (1988) 3098.
[49] A.D. Becke, J. Chem. Phys. 98 (1993) 5648.
[50] C. Lee, W. Yang, R.G. Parr, Phys. Rev. B 37 (1988) 785.
[51] M.J. Frisch, G.W. Trucks, H.B. Schlegel, G.E. Scuseria, M.A. Robb, J.R. Cheeseman, V.G. Zakrzewski, J.A. Montgomery Jr., R.E. Stratmann, J.C. Burant, S. Dapprich, J.M. Millam, A.D. Daniels, K.N. Kudin, M.C. Strain, O. Farkas, J. Tomasi, V. Barone, M. Cossi, R. Cammi, B. Mennucci, C. Pomelli, C. Adamo, S. Clifford, J. Ochterski, G.A. Petersson, P.Y. Ayala, Q. Cui, K. Morokuma, P. Salvador, J.J. Dannenberg, D.K. Malick, A.D. Rabuck, K. Raghavachari, J.B. Foresman, J. Cioslowski, J.V. Ortiz, A.G. Baboul, B.B. Stefanov, G. Liu, A. Liashenko, P. Piskorz, I. Komaromi, R. Gomperts, R.L. Martin, D.J. Fox, T. Keith, M.A. Al-Laham, C.Y. Peng, A. Nanayakkara, M. Challacombe, P.M.W. Gill, B. Johnson, W. Chen, M.W. Wong, J.L. Andres, C. Gonzalez, M. Head-Gordon, E.S. Replogle, J.A. Pople, Gaussian 98 (Rev. A. 11), Gaussian, Inc., Pittsburgh, PA, 2001.
[52] N. Godbout, D.R. Salahub, J. Andzelm, E. Wimmer, Can. J. Chem. 70 (1992) 560.
[53] N.Godbout, "Ensemble de base pour la théorie de la fonctionnelle de la densité - Structures moléculaires, propriétés mono-électroniques et modèles de zéolites", Département de chimie, Faculté des arts et des sciences, Université de Montréal, 1996.
[54] C. Gonzalez, H.B. Schlegel, J. Chem. Phys. 90 (1989) 2154.